

An Energy-Conserved Calibration System for Microwave Instruments

Fuzhong Weng¹, Yang Han¹ and Zhengzhan Wang²

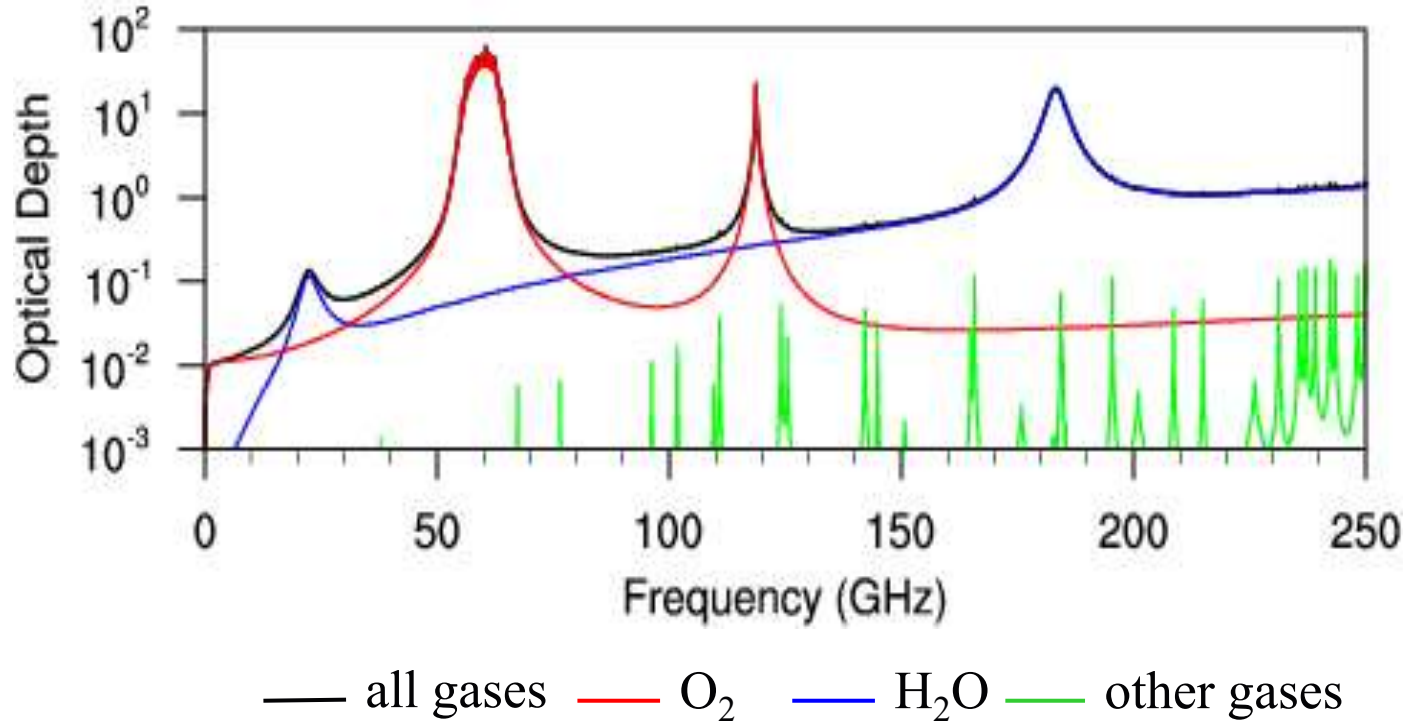
1. Center for Earth System Modeling and Prediction, Beijing, China
2. Chinese Space Science Center, Beijing, China

25th International TOVS Study Conference, GOA, India, May 8-13, 2025

Outline

- **Impacts from Uses of Microwave Data in Weather and Climate Studies**
- **Current Approaches for Microwave Instrument Calibration**
- **An Energy-Conserved Calibration System (ECCS)**
- **ECCS Consensus with Polarimetric Radiative Transfer Theory**
- **Summary and Conclusions**

Microwave Absorption Spectroscopy



The frequencies from 20 to 200 GHz are often used for microwave sounders. The future missions will consider more frequencies above 200 GHz

Detailed O₂ Absorption Spectroscopy between 50-70 GHz

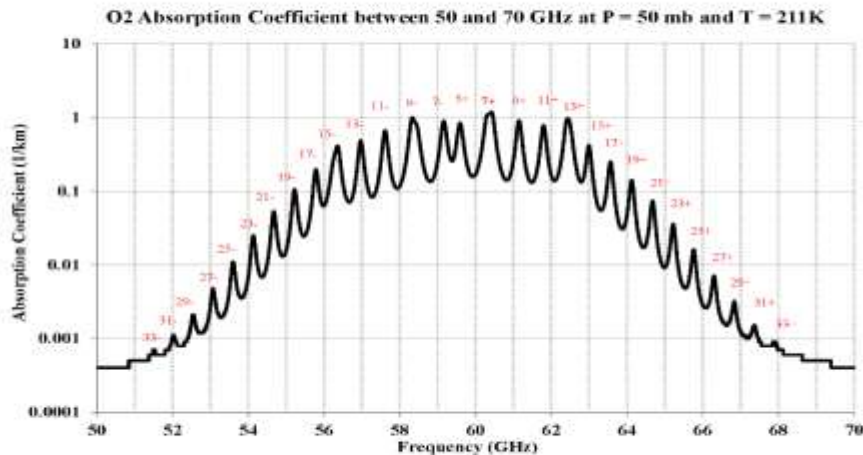
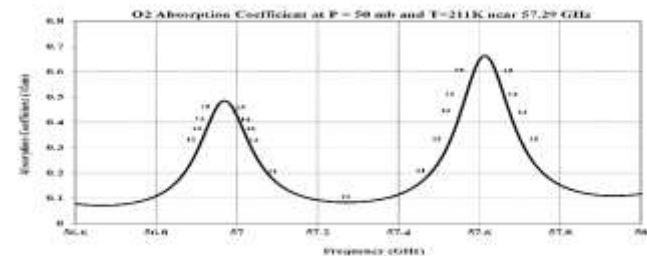


Table 2.1 Frequency location with the magnetic dipole quantum number.

N-	Frequency	N+	Frequency
1-	118.7503	1+	56.2648
3-	62.4863	3+	58.4466
5-	60.3061	5+	59.5910
7-	59.1642	7+	60.4348
9-	58.3239	9+	61.1506
11-	57.6125	11+	61.8002
13-	56.9682	13+	62.4112
15-	56.3634	15+	62.9980
17-	55.7838	17+	63.5685
19-	55.2214	19+	64.1278
21-	54.6712	21+	64.6789
23-	54.1300	23+	65.2241
25-	53.5958	25+	65.7648
27-	53.0670	27+	66.3021
29-	52.5424	29+	66.8368
31-	52.0215	31+	67.3695
33-	51.5034	33+	67.9008

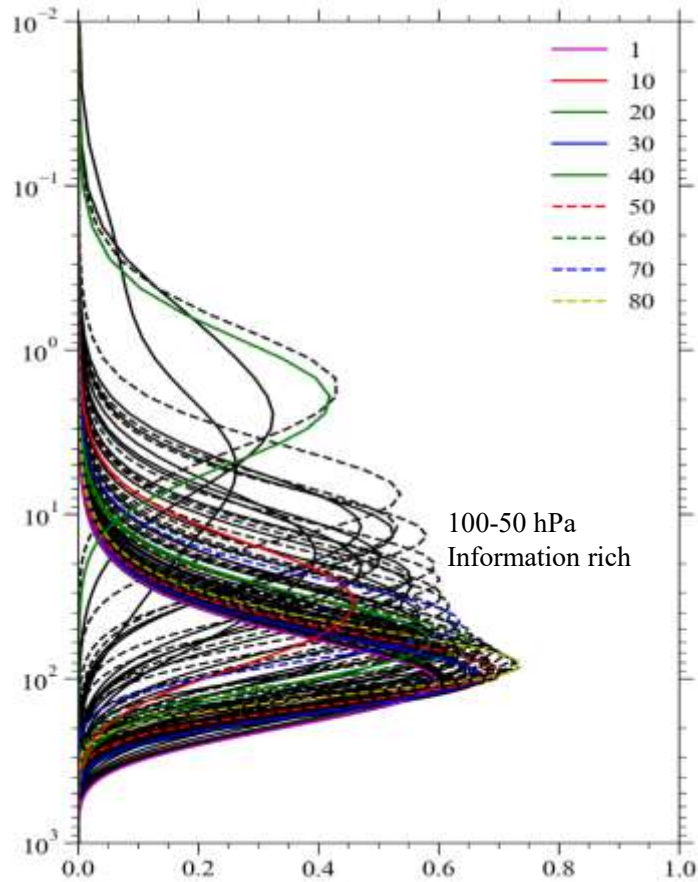
Oxygen absorption coefficients between 50-70 GHz at pressure of 50 mb and temperature of 211 K. Labeled in numeric are the resonant frequency locations where the magnetic-dipole transitions occur with +sign for quantum number J from N to N+1 and -sign for N to N-1.



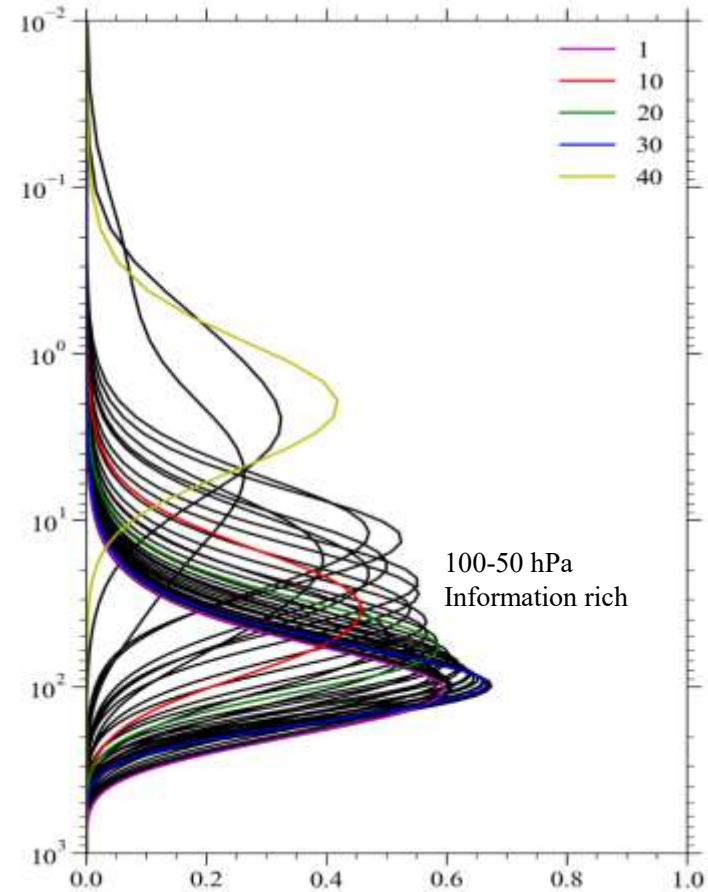
Weng, 2017, Passive Microwave Remote Sensing of the Earth for Meteorological Applications, *Wiley Inc.*

Weighting Functions near 13-O_2 (56.9682 GHz)

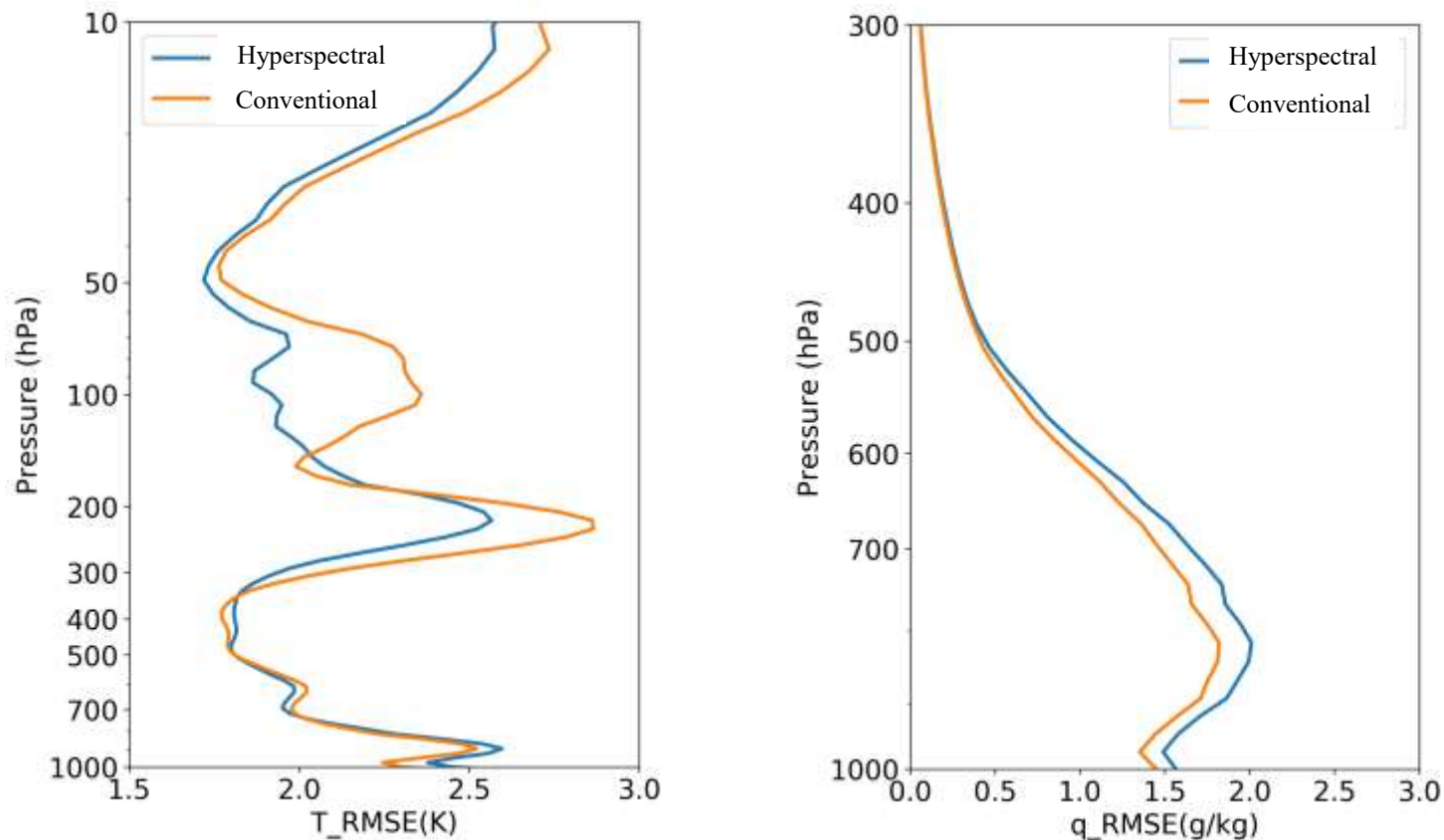
Left side of absorption line



Right side of absorption line



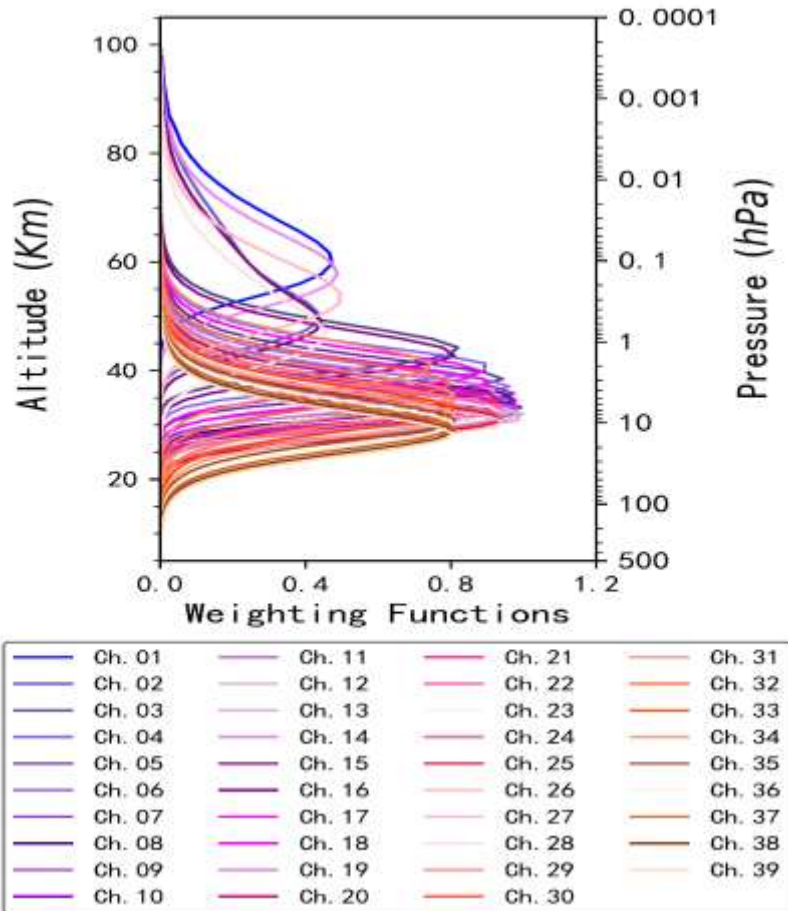
Retrieval Experiments from Microwave Hyperspectral vs Conventional Sounders



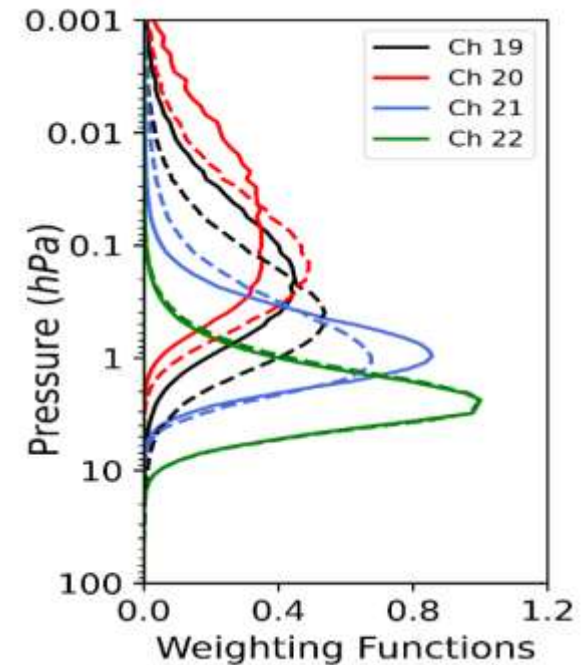
Zhang, Y., **Weng, F.**, Hu H., 2025: Unraveling the Impacts of Hyperspectral Microwave and Terahertz Sounding Channels on Temperature and Humidity Profile Retrieval, *J. Meteorological Research (in press)*

Upper-Air Microwave Sounder

HMAS



SSMIS UAS



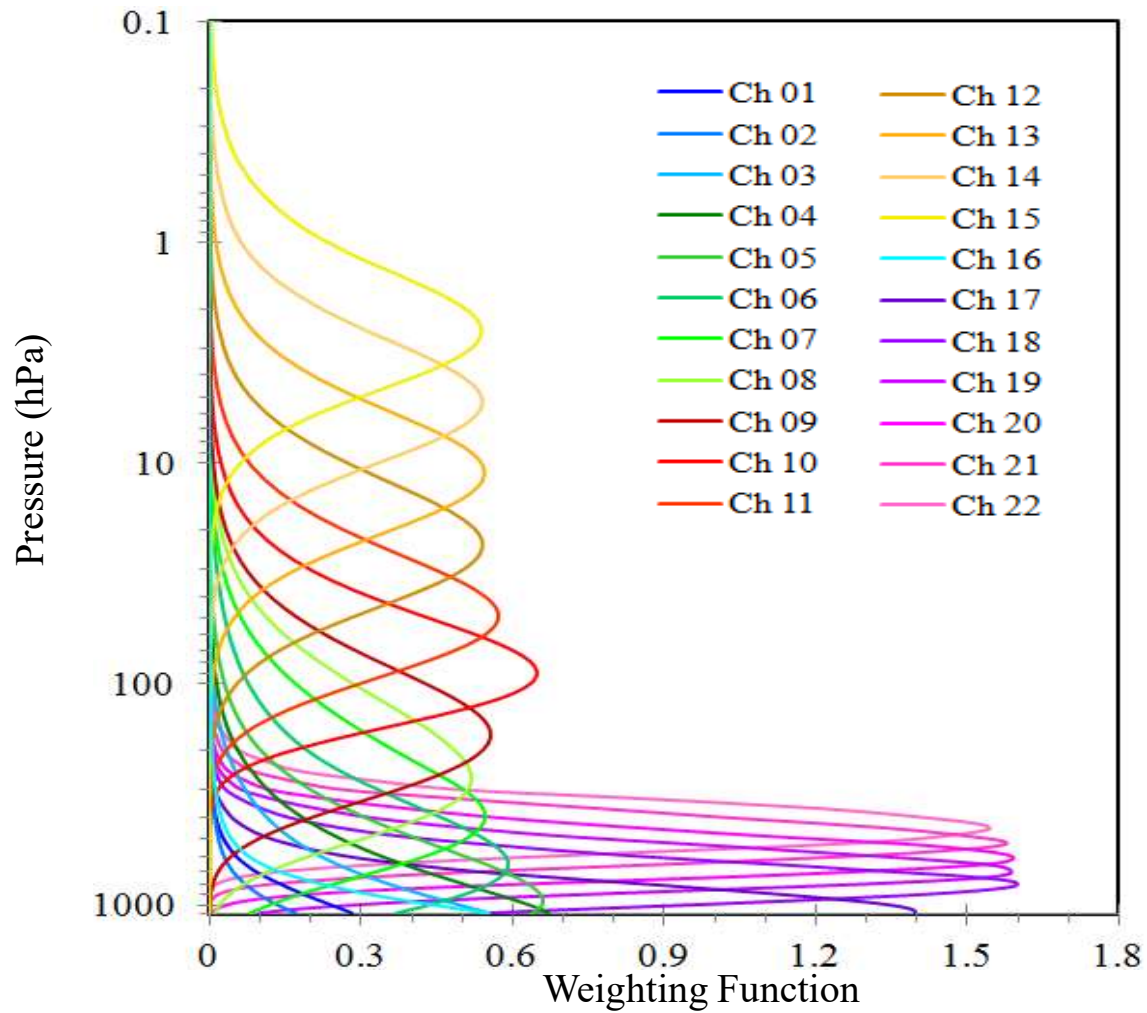
Current SSMIS UAS channel weighting functions, solid line for the geomagnetic field intensity at $B_e = 0.23$ Gauss and dash line for $B_e = 0.63$ Gauss

HMAS has 39 channels and cover 200-0.001 hPa(12-95 km)

ATMS Instrument Characterization

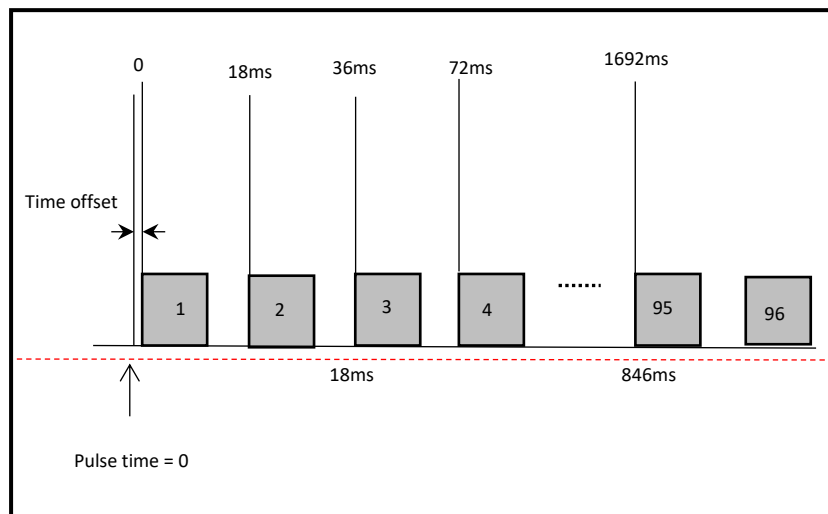
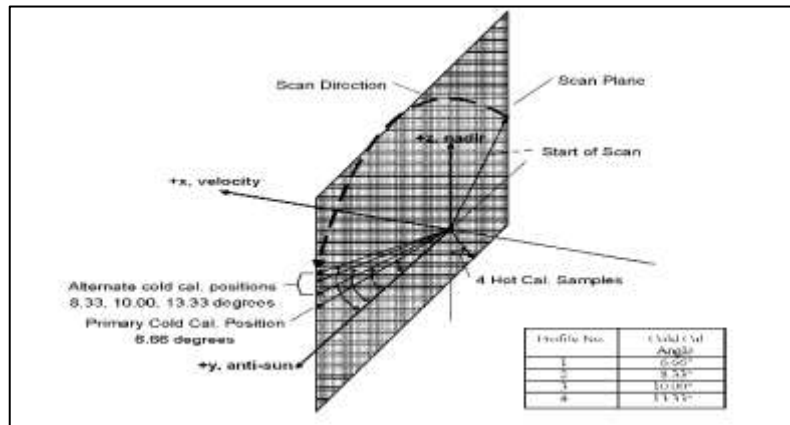
Ch	Channel Central Freq. (MHz)	Polarization	Bandwidth Max. (MHz)	Frequency Stability (MHz)	Calibration Accuracy (K)	Nonlinearity Max. (K)	NEAT (K)	3-dB Bandwidth (deg)	Remarks	Characterization at Nadir
1	23800	QV	270	10	1.0	0.3	0.5	5.2	AMSU-A2	Window-water vapor 100 mm
2	31400	QV	180	10	1.0	0.4	0.6	5.2	AMSU-A2	Window-water vapor 500 mm
3	50300	QH	180	10	0.75	0.4	0.7	2.2	AMSU-A1-2	Window-surface emissivity
4	51760	QH	400	5	0.75	0.4	0.5	2.2		Window-surface emissivity
5	52800	QH	400	5	0.75	0.4	0.5	2.2	AMSU-A1-2	Surface air
6	53596 ± 115	QH	170	5	0.75	0.4	0.5	2.2	AMSU-A1-2	4 km ~ 700 mb
7	54400	QH	400	5	0.75	0.4	0.5	2.2	AMSU-A1-1	9 km ~ 400 mb
8	54940	QH	400	10	0.75	0.4	0.5	2.2	AMSU-A1-1	11 km ~ 250 mb
9	55500	QH	330	10	0.75	0.4	0.5	2.2	AMSU-A1-2	13 km ~ 180 mb
10	57290.344(f_0)	QH	330	0.5	0.75	0.4	0.75	2.2	AMSU-A1-1	17 km ~ 90 mb
11	$f_0 \pm 217$	QH	78	0.5	0.75	0.4	1.0	2.2	AMSU-A1-1	19 km ~ 50 mb
12	$f_0 \pm 322.2 \pm 48$	QH	36	1.2	0.75	0.4	1.0	2.2	AMSU-A1-1	25 km ~ 25 mb
13	$f_0 \pm 322.2 \pm 22$	QH	16	1.6	0.75	0.4	1.5	2.2	AMSU-A1-1	29 km ~ 10 mb
14	$f_0 \pm 322.2 \pm 10$	QH	8	0.5	0.75	0.4	2.2	2.2	AMSU-A1-1	32 km ~ 6 mb
15	$f_0 \pm 322.2 \pm 4.5$	QH	3	0.5	0.75	0.4	3.6	2.2	AMSU-A1-1	37 km ~ 3 mb
16	88200	QV	2000	200	1.0	0.4	0.3	2.2	89000	Window H ₂ O 150 mm
17	165500	QH	3000	200	1.0	0.4	0.6	1.1	157000	H ₂ O 18 mm
18	183310 ± 7000	QH	2000	30	1.0	0.4	0.8	1.1	AMSU-B	H ₂ O 8 mm
19	183310 ± 4500	QH	2000	30	1.0	0.4	0.8	1.1		H ₂ O 4.5 mm
20	183310 ± 3000	QH	1000	30	1.0	0.4	0.8	1.1	AMSU-B/MHS	H ₂ O 2.5 mm
21	183310 ± 1800	QH	1000	30	1.0	0.4	0.8	1.1		H ₂ O 1.2 mm
22	183310 ± 1000	QH	500	30	1.0	0.4	0.9	1.1	AMSU-B/MHS	H ₂ O 0.5 mm

ATMS Channel Weighting Functions

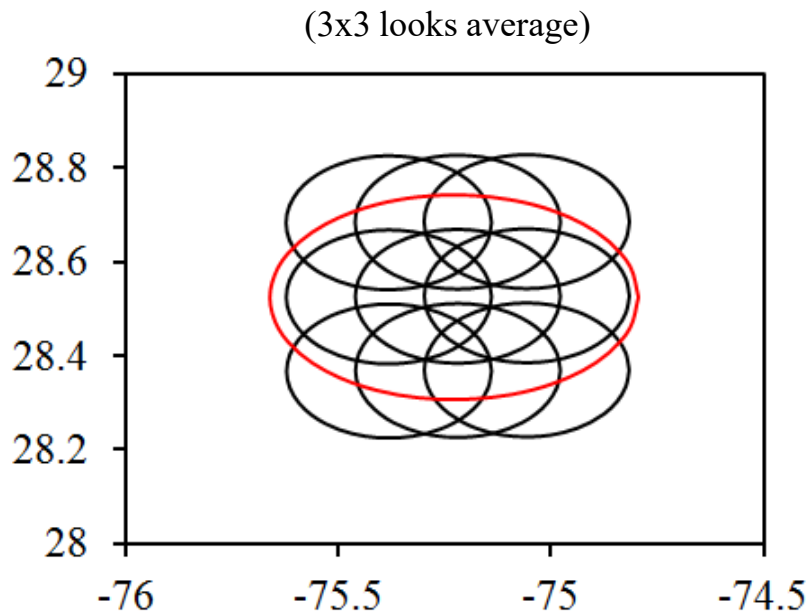


ATMS Scan Profile

Name		Value
Satellite Altitude (km) and inclination angle		824, sun-synch (i=98.7 deg), 1:30 pm Ascending Node
Ground Speed (km/s)		7.0
Scan Period (s)		8/3
Earth View Scan Rate (degree/s)		61.6
Earth View Scan Time (s)		1.728
FOVs/Scan		96
Angular Sample Int (deg)		1.1
Sampling Time (ms)		18.0
Integration Time (ms)		17.6
Nadir EFOV Size (km)	K/Ka	91x75
	V/W	47x32
	G	32x16



ATMS NEDT Reduction through Resampling



Red : AMSU FOV or CRIS FOR near nadir
Black: ATMS FOV near nadir

Noise for single
observation

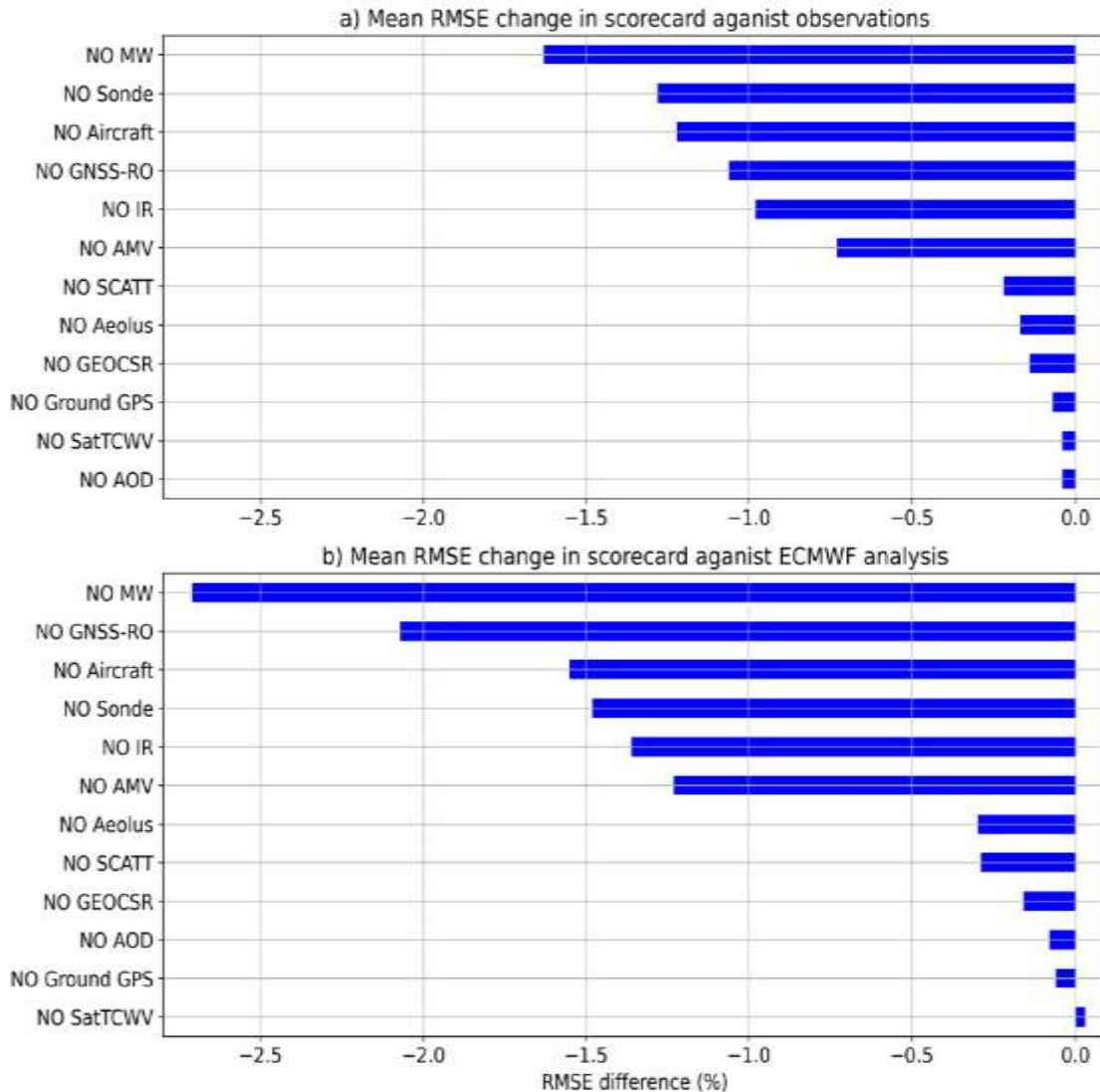
$$NE\Delta T = \frac{T_{sys}}{\sqrt{B \cdot \tau}}$$

**Noise after average over
multiple looks**

$$NE\Delta T = \frac{T_{sys}}{3 \cdot \sqrt{B \cdot \tau}}$$

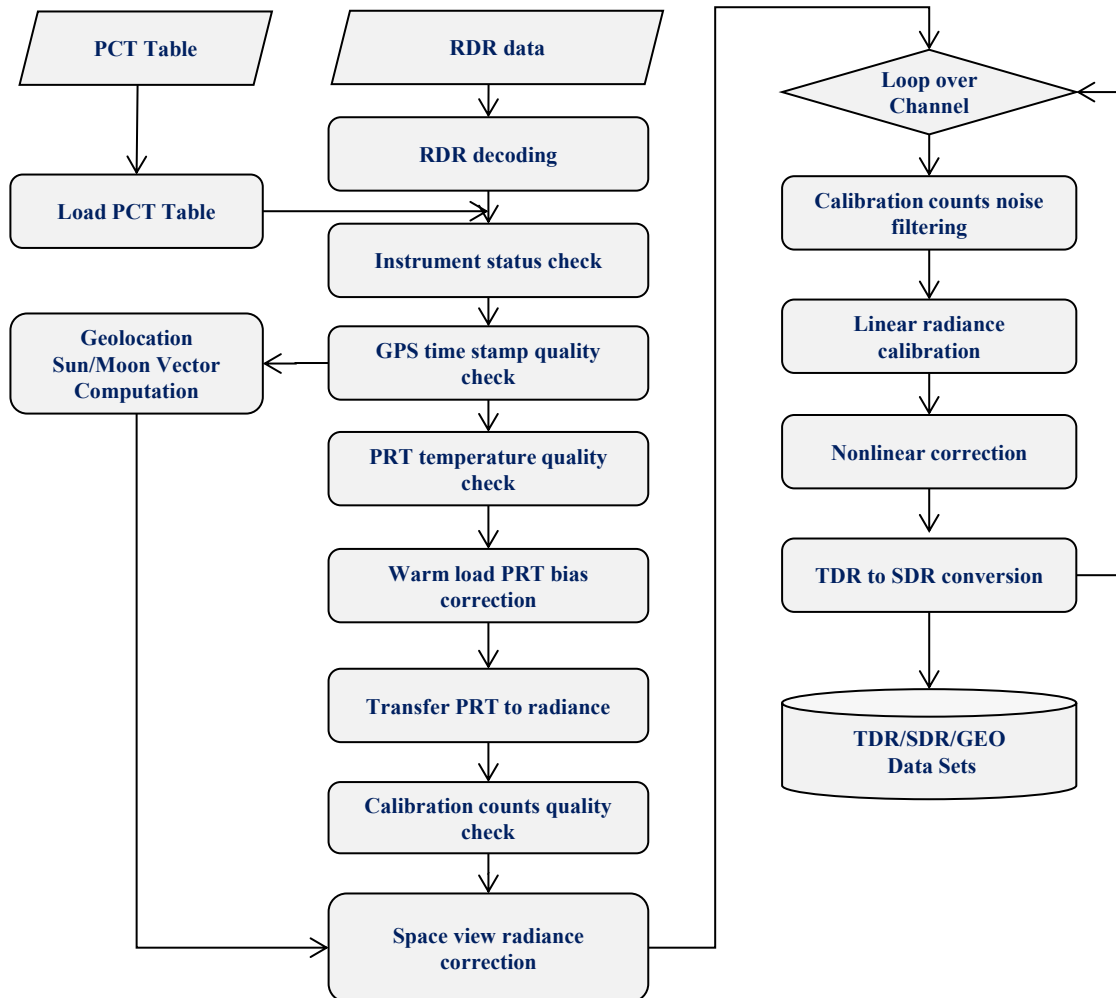
Impacts of Microwave Data on Global Weather Forecasts

(WMO 8th impact workshop,2024)



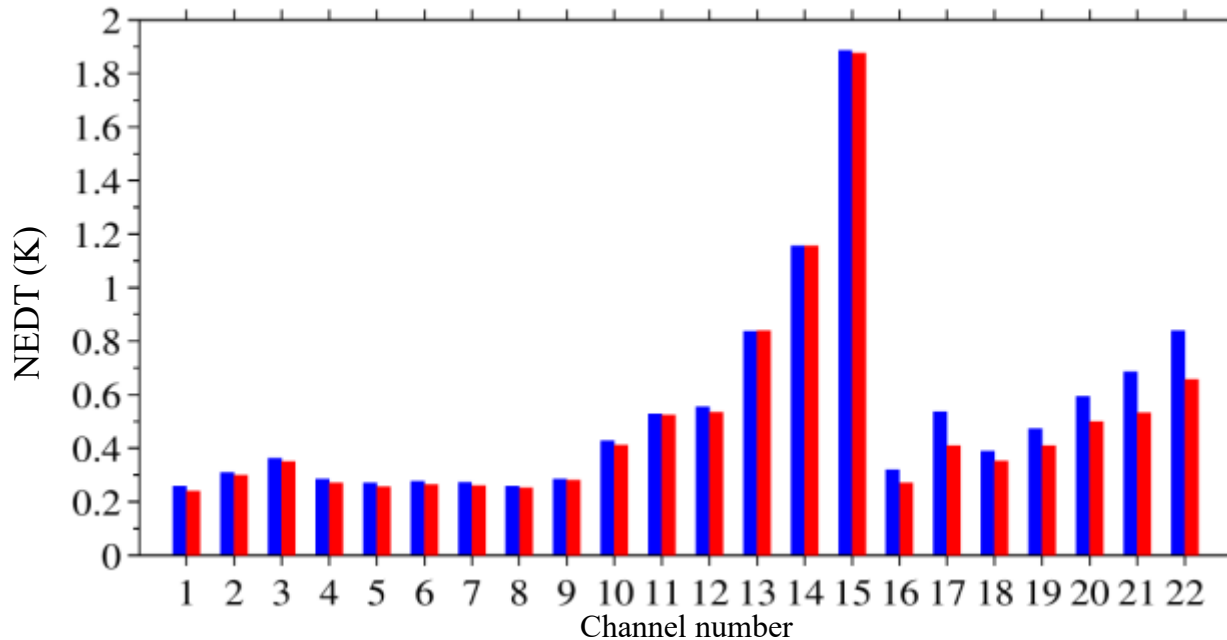
- MW Sounders, GNSS-RO, sondes and aircraft give the large impact.
- GNSS-RO overtakes the IR.
- AMV is also important.
- On average all the observing network shows the beneficial impact on the forecast.

Suomi NPP ATMS RDR to TDR Processing Diagram



- Radiation from calibration targets are calculated as radiance instead of brightness temperature
- Lunar contamination correction is included in space view radiance correction
- Nonlinearity correction is based on “ μ ” parameter derived from TVAC
- Brightness temperature is computed from full Planck function in radiance space
- Error budget in calibration are traceable

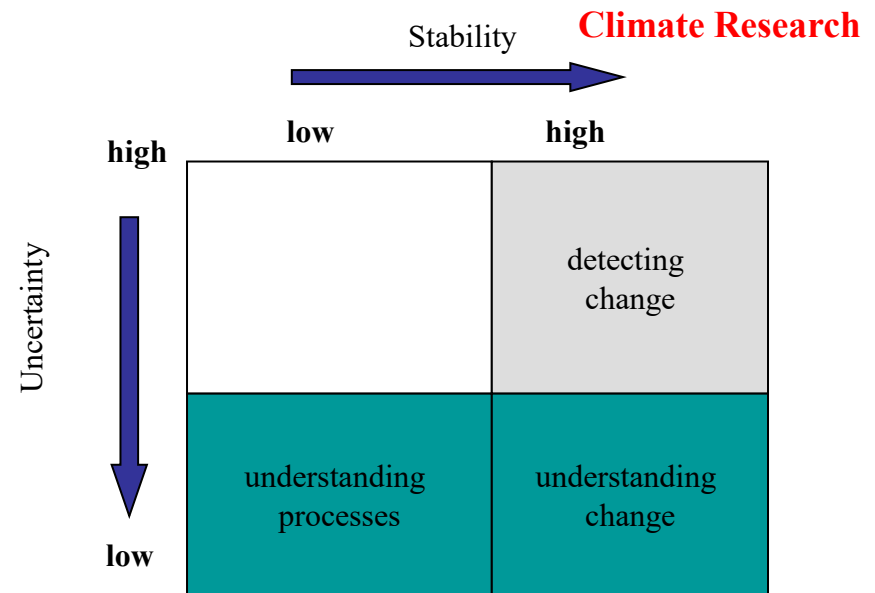
ATMS NEDT Computed from Standard and Allan Deviations



ATMS standard deviation (blue) and Allan deviation (red) with channel number. The sample size (N) is 150 and the averaging factor (m) for the warm counts is 17. The standard deviation is much higher than Allan deviation.

Requirements on Satellite Data for Weather and Climate Applications

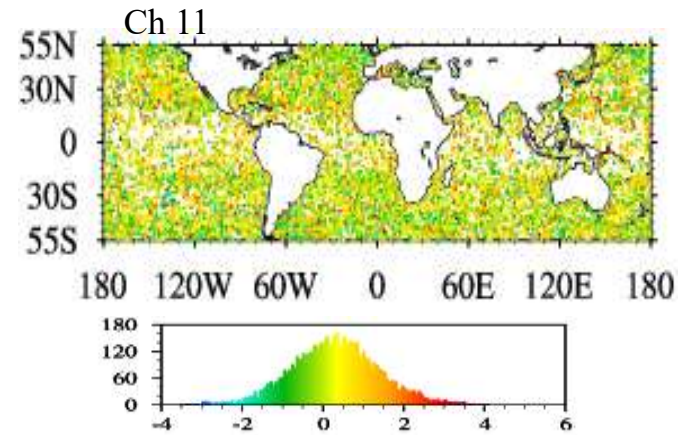
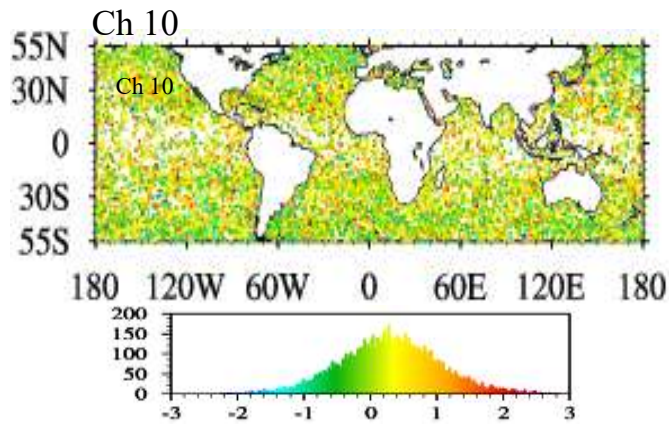
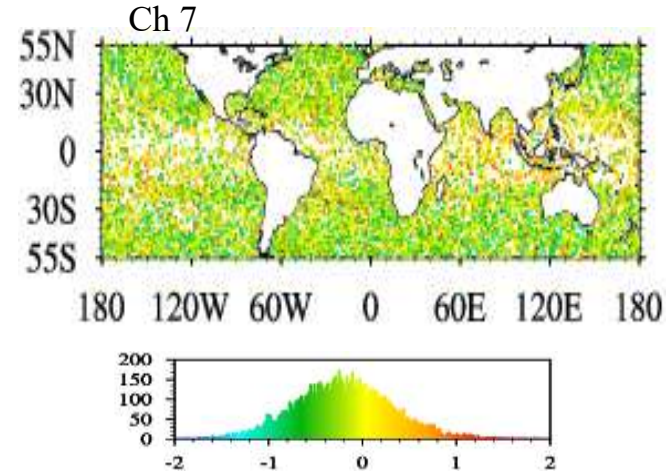
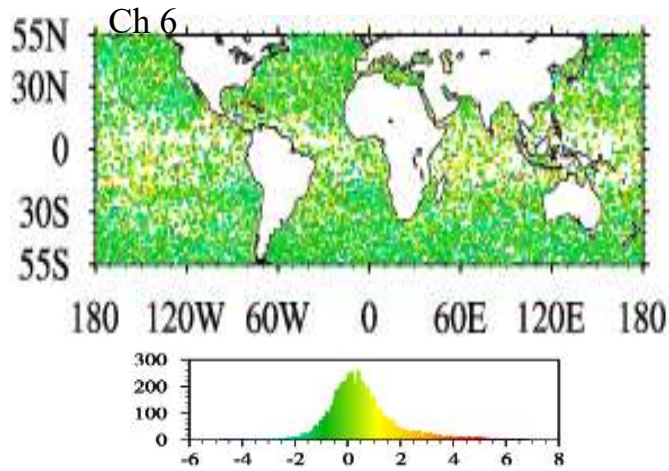
- **Accuracies versus stabilities**
 - For measuring long-term trend: accuracy not critical - stability important
 - For understanding climate: accuracy critical
 - Stability appears to be less difficult to achieve in satellite instruments
- **Stability criterion**
 - 1/5 of decadal climate signal (somewhat arbitrary)
 - Implies uncertainty range of 0.8 to 1.2, or factor of 1.5, for unit change
 - Climate model predictions differ by factor of 4 (temperature increase of 1.4 to 5.8 K by 2100)
 - Stability of 1/5 of signal would lead to considerable narrowing of possible climate model scenarios
 - Presence of natural climate variability will increase uncertainty in detected signal and lengthen time required to detect signal



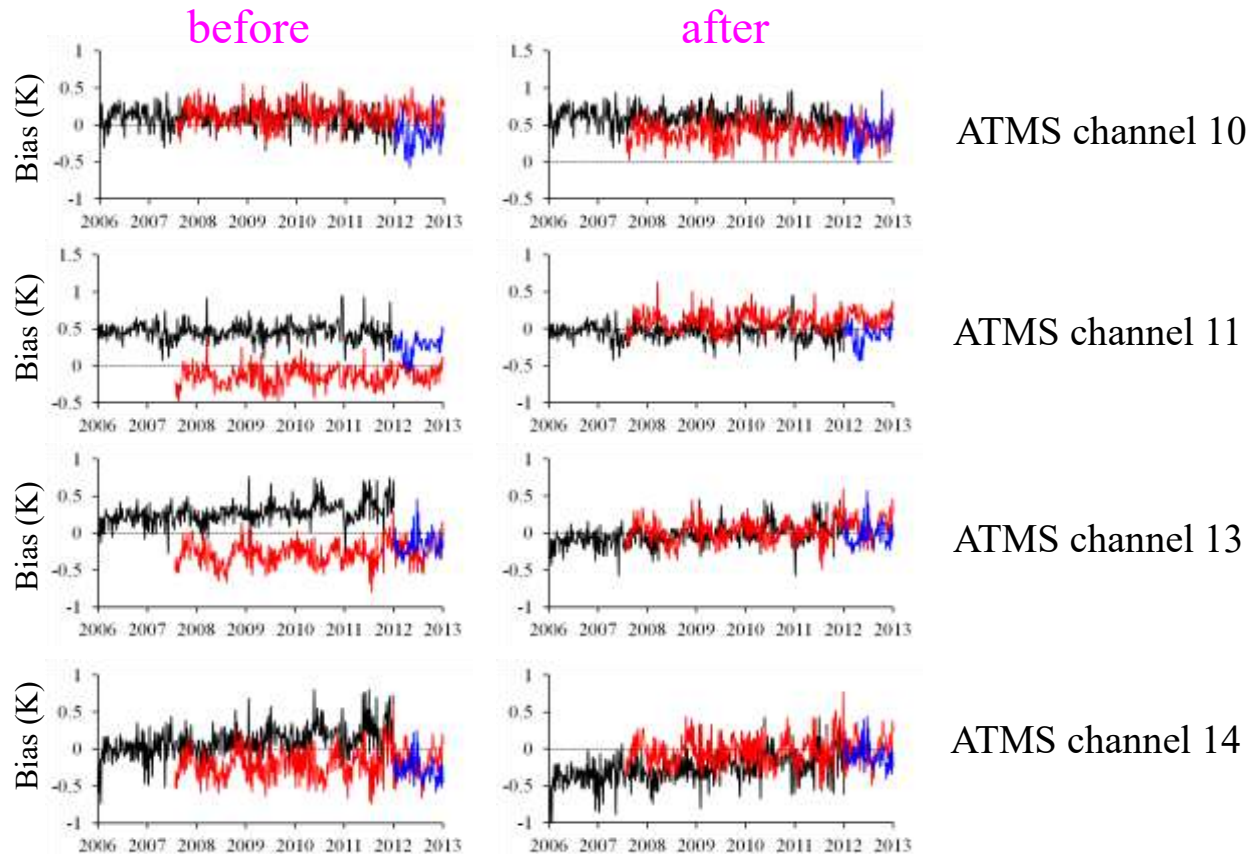
Weather Forecasting

(Graeme Stephens, 2003)

ATMS Bias Obs (TDR) - GPS Simulated



Cross-Calibration between AMSU-A and ATMS



The pentad data set within $\pm 30^\circ$ latitudinal band (Red: METOP-A, Black: NOAA-15).
NOAA-18 AMSU-A is used as reference

ATMS Calibration Error Budget Model

The ATMS radiometric calibration for antenna brightness temperature is derived as

$$R = \bar{R}_c + (\bar{R}_w - \bar{R}_c) \left(\frac{C_s - \bar{C}_c}{\bar{C}_w - \bar{C}_c} \right) + Q$$

Q is the calibration non-linearity term:

$$Q = \mu (\bar{R}_w - \bar{R}_c)^2 \frac{(C_s - \bar{C}_w)(C_s - \bar{C}_c)}{(\bar{C}_w - \bar{C}_c)^2} = 4Q_{\max} (x - x^2)$$

Considering the system noise and gain drift errors, the error model for ATMS calibration can be derived as:

$$\Delta R = x\Delta R_w + (1-x)\Delta R_c + 4Q^{\max} (x - x^2) + RMSError \quad x = \frac{C_s - \bar{C}_c}{\bar{C}_w - \bar{C}_c}$$

ΔR_w : error of warm target radiance

ΔR_c : error of cold target radiance

Q^{\max} : maximum nonlinearity $= \frac{1}{4} \cdot \mu \cdot (R_w - R_c)^2$ $\mu = aT^2 + bT + c$

$RMSError$: system noise and gain drift errors

Effects of Emitting Antenna on Scan-Angle Dependent Bias

For Quasi-V (TDR):

$$R_{qv}^c = R_{qv} + \varepsilon_h(R_r - R_h) + [\varepsilon_v(R_r - R_v) - \varepsilon_h(R_r - R_h)]\sin^2 \theta - \frac{R_3}{2}(1 - \varepsilon_h)^{3/2} \sin 2\theta$$

For Quasi-H (TDR):

$$R_{qh}^c = R_{qh} + \varepsilon_h(R_r - R_h) + [\varepsilon_v(R_r - R_v) - \varepsilon_h(R_r - R_h)]\cos^2 \theta + \frac{R_3}{2}(1 - \varepsilon_h)^{3/2} \sin 2\theta$$

The second and third terms are the biases related to the reflector emission

At an incident angle of 45 degree to the plane reflector, the Fresnel equation becomes

$$\varepsilon_v = 2\varepsilon_h - \varepsilon_h^2$$

Weng and Yang, 2024: *Microwave Sounder Calibration and Validation*; Elsevier Inc.

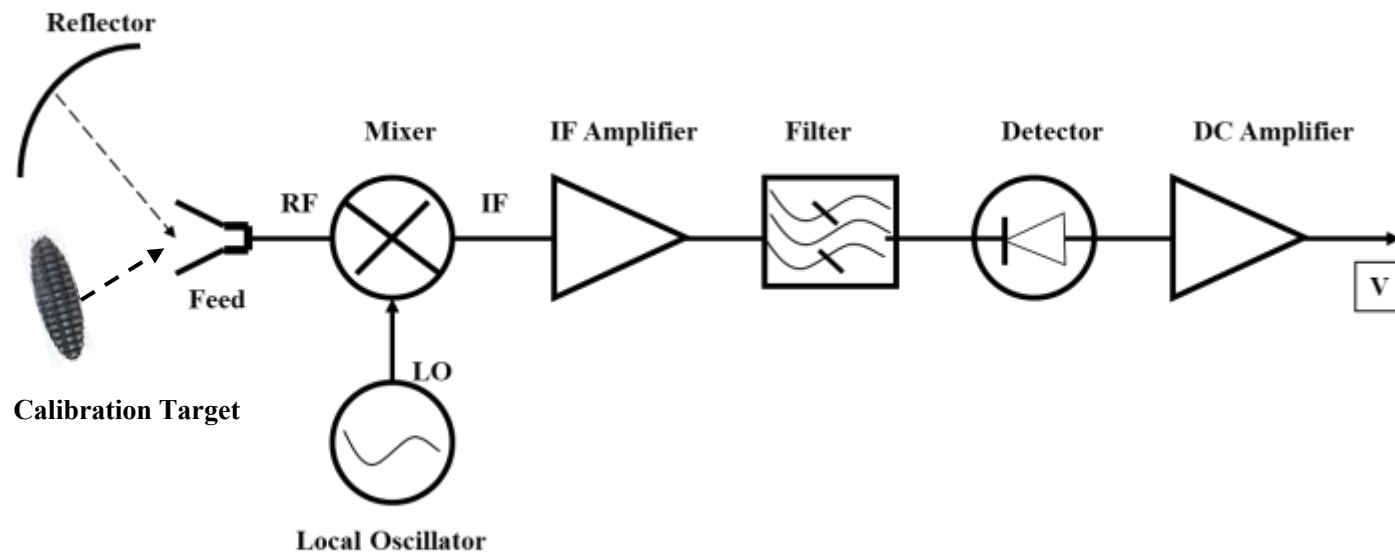
Calibration Accuracy through Deep Space Observations

- On-orbit calibration accuracy derived from pitch maneuver data(using ADL Full Radiance version) compared with those from the PFM error budget model at the cold scene
- The pitch maneuver data at the center location is compared with the truth (2.728K) for defining the on-orbit calibration accuracy

In high frequencies (W,G bands) and cold temperatures, the calibration errors are larger

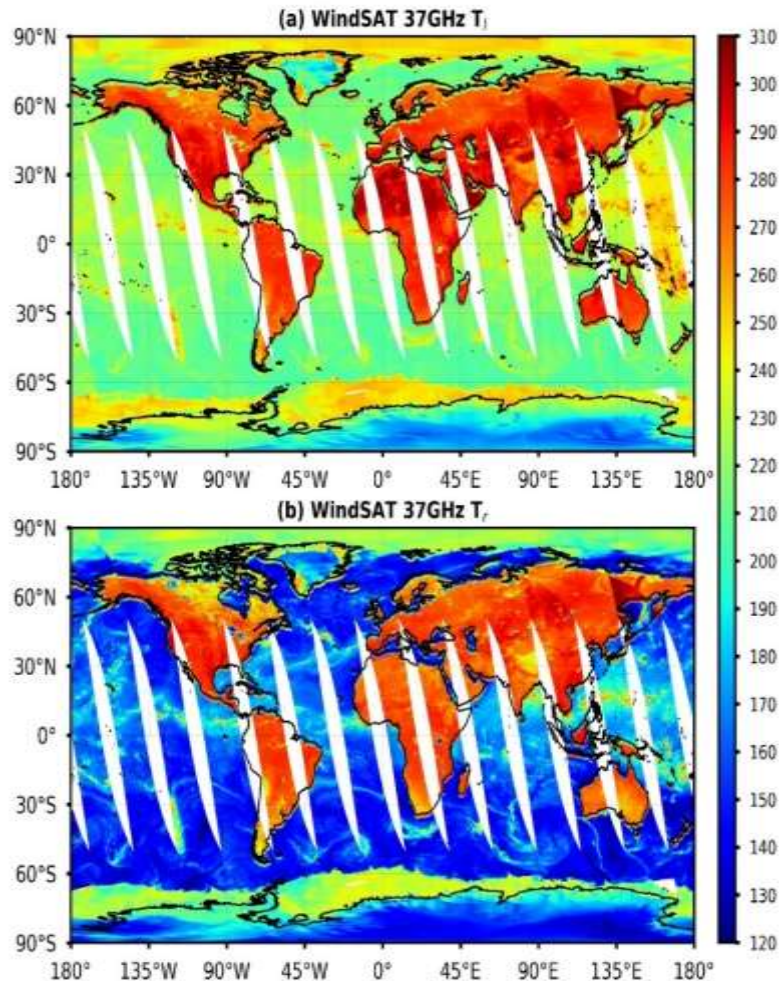
Channel	Scene temperature (K)	
	PFM at 80 K	On-orbit at 2.728K
1	0.265	-0.607
2	0.194	-0.343
3	0.184	0.431
4	0.231	0.498
5	0.224	0.427
6	0.149	0.441
7	0.135	0.553
8	0.225	0.564
9	0.116	0.544
10	0.179	0.653
11	0.240	0.649
12	0.206	0.679
13	0.188	0.723
14	0.132	0.786
15	0.207	0.753
16	0.353	-1.342
17	0.327	1.064
18	0.256	1.342
19	0.291	1.383
20	0.295	1.477
21	0.270	1.429
22	0.289	1.543

A Schematic Diagram of Microwave Radiometer System



Only a single polarization of energy enters into the feedhorn

WindSAT Observations at 37V and 37H



Microwave brightness temperatures over land at both polarization are much warmer than those over oceans due to the large emissivity contrasts and generally over 250 K. In deserts, TBV and TVH are close 300K. According to Stokes vector,

$$I = (I_l, I_r, I_u, I_v)^T \quad I = I_l + I_r, \quad Q = I_l - I_r$$

$$TB = TBV + TBH \approx 600K$$

From a Stoke vector radiative transfer model, we only get about 300K in terms of TB.

What causes this huge discrepancy? Why did we not find this inconsistency in the past?

Inconsistency between Microwave Polarimetric Observations and Radiative Transfer Simulations



Reviewers' comments on GRL paper:

"... more attention should be paid when we use these kinds of polarized measurements. Therefore, I recommend this paper be published as soon as possible, so that scientists working with the microwave could be drawn to attention" (Reviewer 1)

"...The paper is better supported and complemented by the use of several sensors and radiative transfer models. The issue raised by the paper is an important one, well worth discussing in the open literature...." (Dr. Alan Geer, ECMWF Chief Scientist)

Zhu and Weng, 2024, A mystery of the inconsistency between microwave polarimetric observations and radiative transfer simulations, *Geophysical Research Letters*, 10.1029/2024GL111553

Microwave Two-Point Calibration System

In Radiance:

$$R = R_c + (R_w - R_c) \left(\frac{C_s - \overline{C_c}}{C_w - \overline{C_c}} \right) + \mu (R_w - R_c)^2 \frac{(C_s - \overline{C_w})(C_s - \overline{C_c})}{(\overline{C_w} - \overline{C_c})^2}$$

R_w R_c are the radiances of warm and cold calibration targets and defined as follows:

$$R_w(\nu, T_w) = \frac{C_1 \nu^3}{\exp\left(\frac{C_2 \nu}{T_w}\right) - 1} \quad \text{and} \quad R_c(\nu, T_c) = \frac{C_1 \nu^3}{\exp\left(\frac{C_2 \nu}{T_c}\right) - 1}$$

In Brightness Temperature:

$$T_b = T_w + (T_w - T_c) \left(\frac{C_s - \overline{C_w}}{C_w - \overline{C_c}} \right) + \mu (T_w - T_c)^2 \frac{(C_s - \overline{C_w})(C_s - \overline{C_c})}{(\overline{C_w} - \overline{C_c})^2}$$

Rayleigh-Jeans (RJ) Approximation

Assuming $\frac{C_2\nu}{T} \ll 1$, Exponential function in Planck function can be expressed in Taylor series

$$\exp\left(\frac{C_2\nu}{T}\right) = 1 + \frac{C_2\nu}{T} + \frac{1}{2}\left(\frac{C_2\nu}{T}\right)^2 + \dots + \frac{1}{n!}\left(\frac{C_2\nu}{T}\right)^n + \dots$$

Substituting the first-order approximation of the above Taylor expansion into Eq. (5.10) results in the following linear relationship between the blackbody temperature (T)

$$R_\nu^{RJ}(T) = \frac{C_1\nu^2}{C_2} T$$

This is so called Rayleigh–Jeans (RJ) approximation to Planck’s function

$C_2\nu$ is generally less than 10 K for a range of $23.8 \text{ GHz} \leq f \leq 190.3 \text{ GHz}$

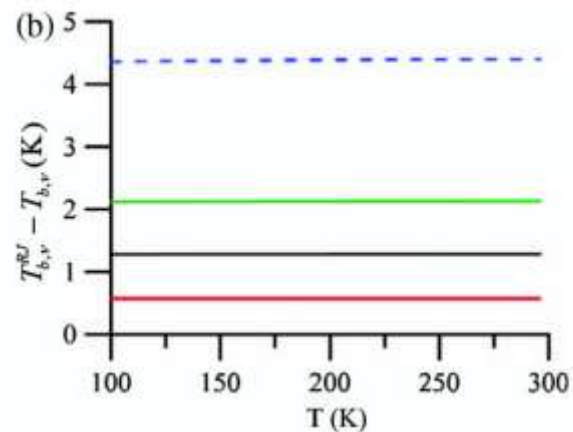
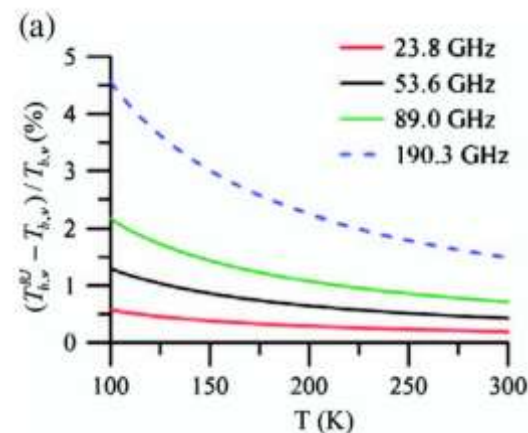
Thus, the temperature in the exponential term must be above 100 K

Two-Point Calibration System in Brightness Temperature

$$T_b = T_w + (T_w - T_c) \left(\frac{C_s - \bar{C}_w}{C_w - \bar{C}_c} \right) + Q_b$$

$$Q_b = \mu (T_w - T_c)^2 \frac{(C_s - \bar{C}_w)(C_s - \bar{C}_c)}{(C_w - \bar{C}_c)^2}$$

This is a calibration equation expressed in terms of brightness temperature. In **cold** temperature or **higher** frequencies. It is generally not recommended due to the error in RJ approximation.



Weng and Zou, 2013

Energy-Conserved Calibration for Microwave Instruments

$$R = R_c + (R_w - R_c) \left(\frac{C_s - \overline{C_c}}{C_w - \overline{C_c}} \right) + Q$$

$$Q = \mu (R_w - R_c)^2 \frac{(C_s - \overline{C_w})(C_s - \overline{C_c})}{(C_w - \overline{C_c})^2}$$

The Energy Conserved Calibration System (ECCS) should use the radiances from half value of Planck function:

R_w is the radiance of warm calibration target

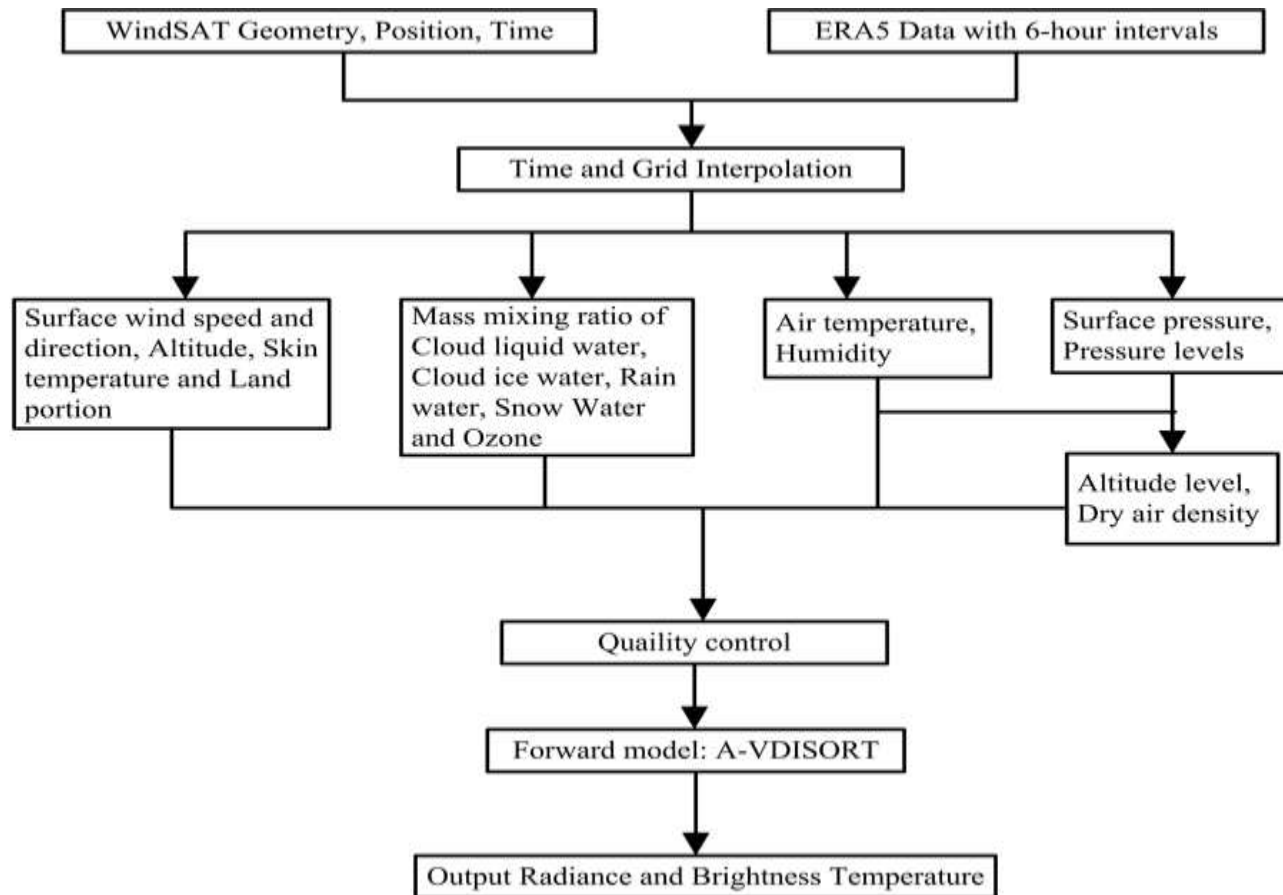
R_c is the radiance of cold calibration target

$$R_w(\nu, T_w) = B(\nu, T_w) / 2.0$$

$$R_c(\nu, T_c) = B(\nu, T_c) / 2.0$$

“The energy received from the microwave radiometer is only contributed from one polarization component.....”, Christian Matzler (Personal communications)

WindSAT Simulations from Vector Radiative Transfer



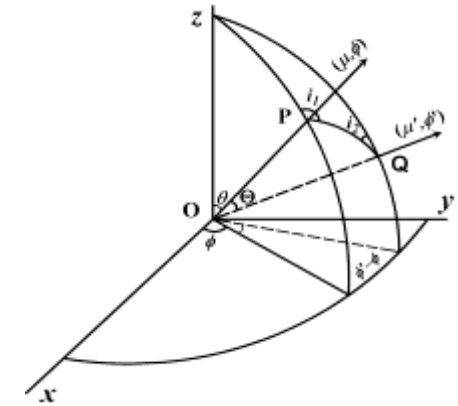
Stokes Vector Radiative Transfer Equation

$$\mu \frac{d\mathbf{I}(\tau, \mu, \phi)}{d\tau} = \mathbf{I}(\tau, \mu, \phi) - \frac{\omega(\tau)}{4\pi} \int_0^{2\pi} d\phi' \int_{-1}^1 \mathbf{M}(\tau, \mu, \phi; \mu', \phi') \mathbf{I}(\tau, \mu', \phi') d\mu' - \mathbf{Q}(\tau, \mu, \phi)$$

$$\mathbf{Q}(\tau, \mu, \phi) = \frac{\omega(\tau)}{4\pi} \mathbf{M}(\tau, \mu, \phi; -\mu_0, \phi_0) \mathbf{S}_b \exp(-\tau / \mu_0) + (1 - \omega(\tau)) \mathbf{S}_t(\tau)$$

where Stokes vector

$$\mathbf{I}(\tau, \mu, \phi) \left\{ \begin{array}{l} (I_l, I_r, I_u, I_v)^T \\ (I, Q, U, V)^T \end{array} \right. \quad I = I_l + I_r, \quad Q = I_l - I_r$$



Thermal source: $\mathbf{S}_t(\tau) = \left(\frac{B[T(\tau)]}{2}, \frac{B[T(\tau)]}{2}, 0, 0 \right)^T$

Beam source: $\mathbf{S}_b = \left(\frac{I_0}{2}, \frac{I_0}{2}, 0, 0 \right)^T$

Phase matrix: $\mathbf{M} = \mathbf{L}(\pi - i_2) \mathbf{S}(\Theta) \mathbf{L}(-i_1)$

For nonspherical particle

$$\mathbf{S} = \begin{bmatrix} S_{11} & S_{12} & S_{13} & S_{14} \\ S_{21} & S_{22} & S_{23} & S_{24} \\ S_{31} & S_{32} & S_{33} & S_{34} \\ S_{41} & S_{42} & S_{43} & S_{44} \end{bmatrix}$$

For spherical particle

$$\mathbf{S} = \begin{bmatrix} S_{11} & 0 & 0 & 0 \\ 0 & S_{22} & 0 & 0 \\ 0 & 0 & S_{33} & S_{34} \\ 0 & 0 & -S_{34} & S_{33} \end{bmatrix}$$

New Vector Discrete-Ordinate Radiative Transfer (VDISORT) Scheme

$$\mu \frac{d}{d\tau} \begin{pmatrix} \mathbf{I}_{m,lr}^c(\tau, \mu_s) \\ \mathbf{I}_{m,uv}^c(\tau, \mu_s) \\ \mathbf{I}_{m,lr}^s(\tau, \mu_s) \\ \mathbf{I}_{m,uv}^s(\tau, \mu_s) \end{pmatrix} = \begin{pmatrix} \mathbf{I}_{m,lr}^c(\tau, \mu_s) \\ \mathbf{I}_{m,uv}^c(\tau, \mu_s) \\ \mathbf{I}_{m,lr}^s(\tau, \mu_s) \\ \mathbf{I}_{m,uv}^s(\tau, \mu_s) \end{pmatrix} - \begin{pmatrix} \mathbf{Q}_{m,lr}^c(\tau, \mu_s) \\ \mathbf{Q}_{m,uv}^c(\tau, \mu_s) \\ \mathbf{Q}_{m,lr}^s(\tau, \mu_s) \\ \mathbf{Q}_{m,uv}^s(\tau, \mu_s) \end{pmatrix} - \sum_{j=-(N+1), j \neq 0}^{N+1} \begin{pmatrix} c_1 \mathbf{M}_{m,11}^c(\tau, \mu_s, \mu_j) & c_1 \mathbf{M}_{m,12}^c(\tau, \mu_s, \mu_j) & -c_2 \mathbf{M}_{m,11}^s(\tau, \mu_s, \mu_j) & -c_2 \mathbf{M}_{m,12}^s(\tau, \mu_s, \mu_j) \\ c_1 \mathbf{M}_{m,21}^c(\tau, \mu_s, \mu_j) & c_1 \mathbf{M}_{m,22}^c(\tau, \mu_s, \mu_j) & -c_2 \mathbf{M}_{m,21}^s(\tau, \mu_s, \mu_j) & -c_2 \mathbf{M}_{m,22}^s(\tau, \mu_s, \mu_j) \\ c_2 \mathbf{M}_{m,11}^s(\tau, \mu_s, \mu_j) & c_2 \mathbf{M}_{m,12}^s(\tau, \mu_s, \mu_j) & c_2 \mathbf{M}_{m,11}^c(\tau, \mu_s, \mu_j) & c_2 \mathbf{M}_{m,12}^c(\tau, \mu_s, \mu_j) \\ c_2 \mathbf{M}_{m,21}^s(\tau, \mu_s, \mu_j) & c_2 \mathbf{M}_{m,22}^s(\tau, \mu_s, \mu_j) & c_2 \mathbf{M}_{m,21}^c(\tau, \mu_s, \mu_j) & c_2 \mathbf{M}_{m,22}^c(\tau, \mu_s, \mu_j) \end{pmatrix} \begin{pmatrix} \mathbf{I}_{m,lr}^c(\tau, \mu_j) \\ \mathbf{I}_{m,uv}^c(\tau, \mu_j) \\ \mathbf{I}_{m,lr}^s(\tau, \mu_j) \\ \mathbf{I}_{m,uv}^s(\tau, \mu_j) \end{pmatrix}$$

$$c_1 = \frac{\omega(\tau)}{4} w_j (1 + \delta_{0m}); \quad c_2 = \frac{\omega(\tau)}{4} w_j (1 - \delta_{0m}); \quad s = -(N+1), \dots, (N+1) \text{ and } s \neq 0$$

$$\mathbf{i}_m(\tau, \mu_s) = \begin{pmatrix} \mathbf{I}_{m,lr}^c(\tau, \mu_s) \\ \mathbf{I}_{m,uv}^c(\tau, \mu_s) \\ \mathbf{I}_{m,lr}^s(\tau, \mu_s) \\ \mathbf{I}_{m,uv}^s(\tau, \mu_s) \end{pmatrix}; \quad \mathbf{q}_m(\tau, \mu_s) = - \begin{pmatrix} \mathbf{Q}_{m,lr}^c(\tau, \mu_s) \\ \mathbf{Q}_{m,uv}^c(\tau, \mu_s) \\ \mathbf{Q}_{m,lr}^s(\tau, \mu_s) \\ \mathbf{Q}_{m,uv}^s(\tau, \mu_s) \end{pmatrix}$$

Zhu, Z., F. Weng, and Y. Han, 2024: Vector radiative transfer in a vertically inhomogeneous scattering and emitting atmosphere. Part I: A new discrete ordinate method. *J. Meteor. Res.*, **38**(2), 209–224, doi: 10.1007/s13351-024-3076-3.

ARMS 2.0 will be based on new VDISORT theory and can be applied for both non-specular surface reflection and non-spherical ice cloud scattering

VDISORT Lower Boundary Scheme

$$\mathbf{I}(\mu, \phi) = \mathbf{E}\mathbf{S}_t + \int_0^{2\pi} \int_0^1 \mathbf{R}(\mu, \phi; -\mu', \phi') \mu' \mathbf{I}(-\mu', \phi') d\mu' d\phi' + \mathbf{R}(\mu, \phi; -\mu_0, \phi_0) \mu_0 \mathbf{S}_b \exp(-\tau_L / \mu_0)$$

where emissivity vector (\mathbf{E}) and BRDF (\mathbf{R}) are related to each other; \mathbf{S}_t and \mathbf{S}_b are thermal Stokes vector and solar Stokes vector respectively

$$\mathbf{R}(\theta^i, \phi^i; \theta^s, \phi^s) = \begin{pmatrix} R_{llll} & R_{lrlr} & \text{Re}(R_{lrll}) & \text{Im}(R_{lrll}) \\ R_{rllr} & R_{rrrr} & \text{Re}(R_{rrrl}) & \text{Im}(R_{rrrl}) \\ 2 \text{Re}(R_{llrl}) & 2 \text{Re}(R_{lrrr}) & \text{Re}(R_{llrr} + R_{lrrl}) & \text{Im}(R_{rrll} + R_{rllr}) \\ 2 \text{Im}(R_{llrl}) & 2 \text{Im}(R_{lrrr}) & \text{Im}(R_{llrr} + R_{lrrl}) & \text{Re}(R_{rrll} - R_{rllr}) \end{pmatrix} \quad \text{Polarized BRDF matrix}$$

$$\mathbf{E}(\mu, \phi) = \mathbf{N} - \int_0^{2\pi} \int_0^1 \mathbf{R}(\mu, \phi; -\mu', \phi') \mu' d\mu' d\phi'$$

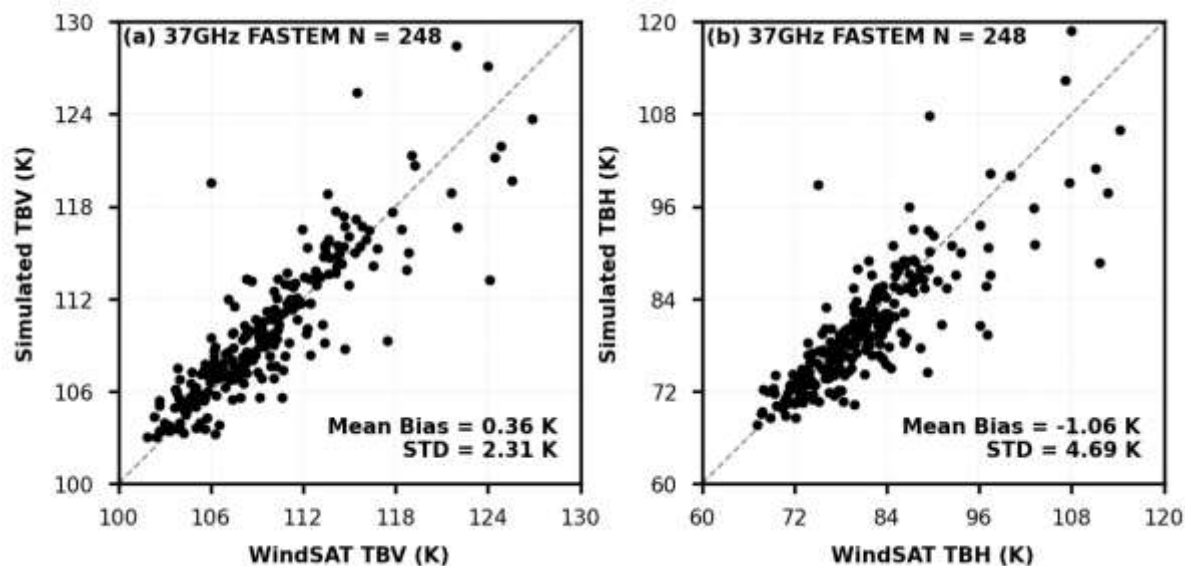
For an absorption surface, Kirchhoff's Law is generalized to compute the emissivity matrix as follows:

Liu, Q. , F. Weng and S. English, 2011: An Improved Fast Microwave Water Emissivity model: *IEEE Trans. Geosci. Remote Sens.*, 1238-1250, DOI: 10.1109/TGRS.2010.2064779.

He, L. and F. Weng, 2023: Improved Microwave Emissivity and Reflectivity Model derived from Two-scale Roughness Theory, *Adv Atmos. Sci.*, 40, 1923-1938

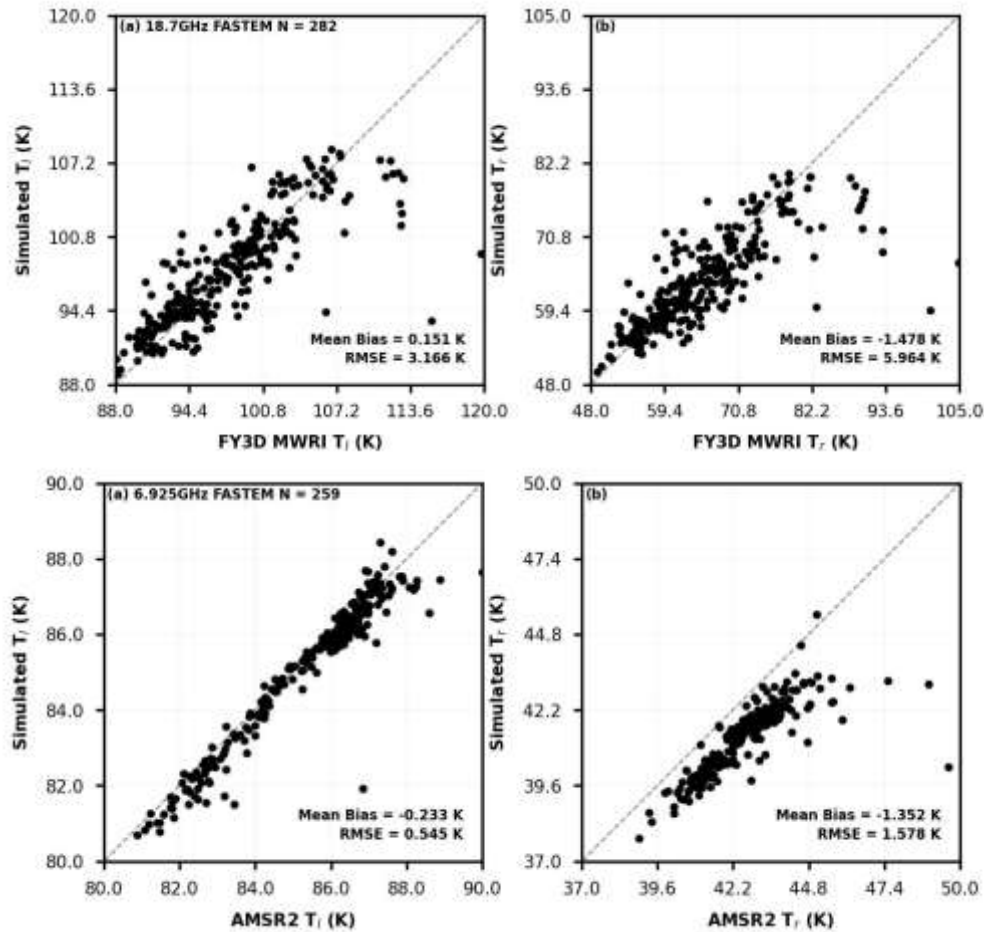
$$\mathbf{R}(\mu_s, \phi_s, \mu_i, \phi_i) = \sum_{m=0}^{\infty} \left\{ \mathbf{R}_m^c(\mu_s, \mu_i, \phi_s) \cos m(\phi_i - \phi_s) + \mathbf{R}_m^s(\mu_s, \mu_i, \phi_s) \sin m(\phi_i - \phi_s) \right\}$$

VDISORT Simulations vs. WindSAT Observations



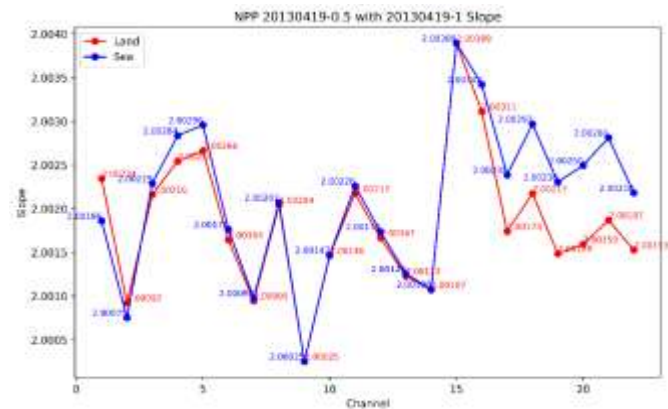
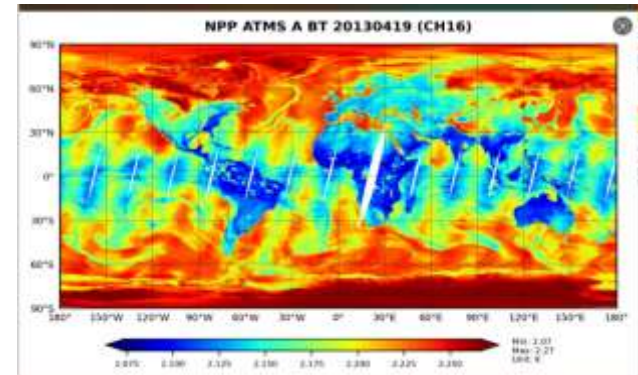
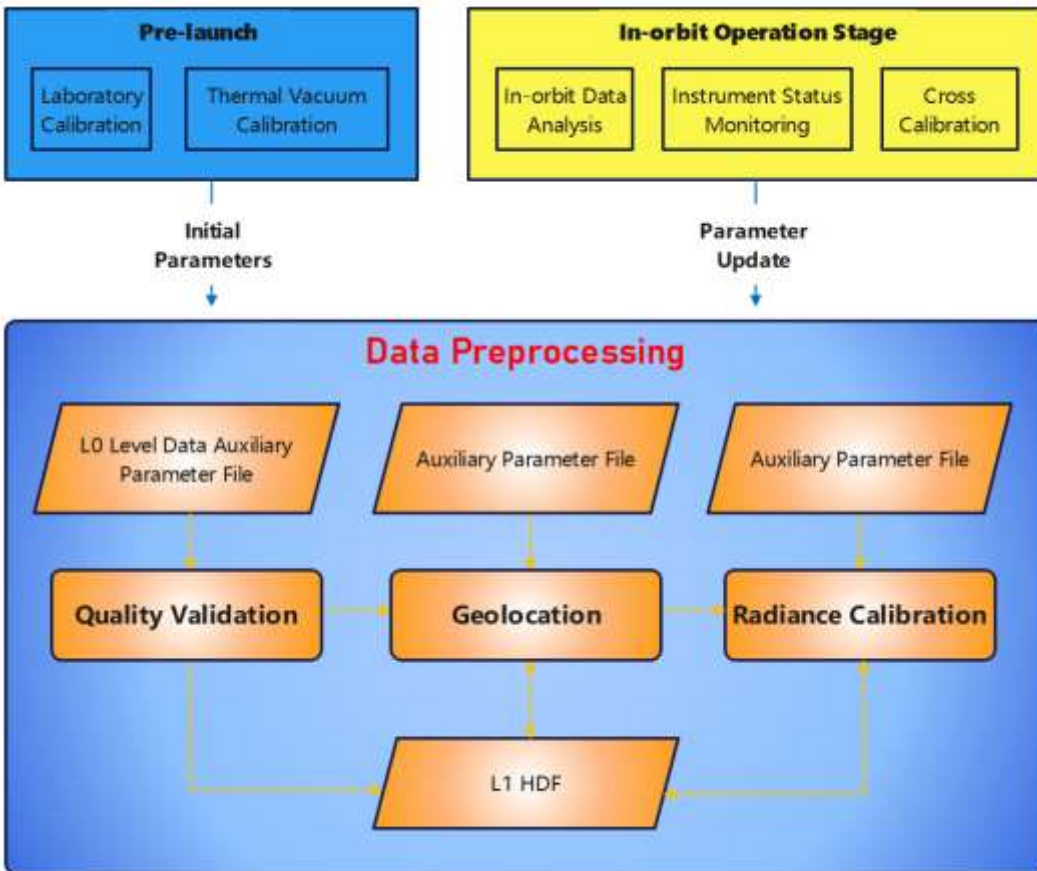
Windsat data are collocated with ERA5 data (Temperature, humidity, hydrometeor profiles, surface temperature, surface wind. Shown are the all sky vertically (left) and horizontally (right) brightness temperatures at 37 GHz simulated with both VDISORT and ARTS. The surface emissivity model is based on FASTEM-6. Notice that Windsat data have been divided by 2 to get a linear relationship with simulations.

VDISORT Simulations vs MWRI and AMSR2 Observations



- Observations are divided by 2
- Ocean Emissivity Mode: FASTEM-6
- Radiative Transfer Model: VDISORT

Energy-Conserved Calibration System (ECCS) for Microwave Radiometers



ATMS data distributed from the operational calibration is about a factor 2 higher than the new calibration result

Can Scalar Radiative Transfer Models Indicate the Inconsistency between Microwave Observations and Simulations?

$$\mu \frac{dI(\tau, \mu, \phi)}{d\tau} = I(\tau, \mu, \phi) - \frac{\omega(\tau)}{4\pi} \int_0^{2\pi} d\phi' \int_{-1}^1 P(\tau, \mu, \phi; \mu', \phi') I(\tau, \mu', \phi') d\mu' - Q(\tau, \mu, \phi)$$
$$Q(\tau, \mu, \phi) = \frac{\omega(\tau)}{4\pi} P(\tau, \mu, \phi; -\mu_0, \phi_0) I_0 \exp(-\tau / \mu_0) + (1 - \omega(\tau)) B(\tau)$$

- Currently, scalar radiative transfer models (e.g. CRTM, RTTOV and ARMS) often use **a full Planck function** to compute **the thermal source term** for simulating the polarization brightness temperature.
- Each polarization component is also calculated separately and the total intensity (e.g. the sum of vertical and horizontal polarization) simulated from the scalar RT models is proportional to **2 folds of thermal source term**. Thus, this practice is **similar** to the **current calibration approach**.
- The energy derived from Stokes first component is **incorrect**.

Summary and Conclusions

- **A thermal source term** in vector radiative transfer model should be specified correctly for simulation of polarization sensitive instruments at microwave frequencies.
- From the current calibration system, simulated radiances from a vector radiative transfer model must be **multiplied by a factor of 2** in order to understand the difference (O-B). This factor is now made in the well-known RT models such as ARTS and VDISORT.
- While simulated microwave radiances from the **scalar radiative transfer models** (CRTM, RTTOV, ARMS) can be directly used for diagnosing O-B difference But the scalar radiative transfer models generally does not reflect the interaction of polarization components and result **in some additional biases** in anisotropic atmospheric scattering and surface roughness conditions.
- For the instruments **calibrated in brightness temperature space**, the calibration errors are larger in cold temperatures and higher frequencies.
- In lower frequencies and scattering-free atmosphere, the brightness temperatures from the current calibration system can be inverted to the values from the energy conserved calibration system **by a factor of 2 difference**.
- It is recommended that the future microwave calibration system be designed at **radiance space and be energy conserved** (Alan Geer, ECMWF Chief Scientist).